Fracture Detection in Bio-Glues with Fluorescent-Protein-Based Optical Force Probes

Zhou, Yu; Centeno, Silvia P.; Zhang, Kuan; Zheng, Lifei; Göstl, Robert; Herrmann, Andreas

Published in:
Advanced materials

DOI:
10.1002/adma.202210052

Publication date:
2023

ADVANCED MATERIALS
www.advmat.de

Fracture Detection in Bio-Glues with Fluorescent-Protein-Based Optical Force Probes

Yu Zhou, Silvia P. Centeno, Kuan Zhang, Lifei Zheng, Robert Göstl, and Andreas Herrmann**

Glues are being used to bond, seal, and repair in industry and biomedicine. The improvement of gluing performance is hence important for the development of new glues with better and balanced property spaces, which in turn necessitates a mechanistic understanding of their mechanical failure. Optical force probes (OFPs) allow the observation of mechanical material damage in polymers from the macro- down to the microscale, yet have never been employed in glues. Here, the development of a series of ratiometric OFPs based on fluorescent-protein–dye and protein–protein conjugates and their incorporation into genetically engineered bio-glues is reported. The OFPs are designed to efficiently modulate Förster resonance energy transfer upon force application thereby reporting on force-induced molecular alterations independent of concentration and fluorescence intensity both spectrally and through their fluorescence lifetime. By fluorescence spectroscopy in solution and in the solid state and by fluorescence lifetime imaging microscopy, stress concentrations are visualized and adhesive and cohesive failure in the fracture zone is differentiated.

1. Introduction

Glues are widely used in both industry and biomedicine for applications from object bonding[1] over crevices sealing[2,3] to tissue repair[4,5] and drug delivery.[6,7] These complex environments of application require the development of glues with similarly diverse properties.[8] Therefore, a continuous improvement of glue performance is necessary but presupposes the mechanistic understanding of the inevitable gluing failure. Yet, in practice, it is difficult to predict or detect where and how a glue will fail using traditional methods, for example, as specific cohesive failure within the glue or near the adhesive substrate–glue interface. Cases consisting of multiple failure models in realistic scenarios complicate this situation even further.[9]

In the field of polymer mechanochemistry[10,11] OFPs[12,13] allow the optical visualization and monitoring of mechanically induced events on different length scales within various material systems ranging from traditional thermosets and thermoplastics[14–18] to proteins.[19–23] Similar concepts can be found in the field of mechanobiology as well.[24–27] Upon force application, OFPs undergo conformational, configurational, or constitutional bond isomerization reactions thus altering their optical properties in absorption, fluorescence, or chemiluminescence.[28] The advent of high-resolution microscopy techniques in materials science even enables us to follow macroscopic material damage down to the sub-micrometer scale.[29–37] Thereby, OFPs contribute to the development of approaches for materials with improved properties.[38] While OFPs have thus been successfully employed to investigate damage in both synthetic and biomacromolecular materials, the failure of adhesives surprisingly has not yet been examined using OFPs. Existing methods to investigate the fatigue and fracture[39] of adhesives cover visual inspection,[40] X-ray photoelectron spectroscopy,[41,42] mass spectrometry (MS),[43,44] Fourier-transform infrared spectroscopy,[42,45] and contact angle measurements.[42] Yet, none of these techniques grant spatially resolved optical feedback over the mechanical state of the glue components.

We here report a bio-glue formed by the electrostatic coacervation of cationic force-responsive protein Förster resonance energy transfer (FRET) pairs and anionic aromatic surfactants.[46,47] Therefore, we connect a FRET donor fluorophore to a force-responsive FRET acceptor fluorescent protein. The FRET efficiency, and thereby the emission spectrum as well as donor fluorescence lifetime, is altered by force application during mechanical testing. We use these protein adhesives to glue both high-energy and low-energy surfaces for the detailed optical analysis of their fracture behavior. Mechanical damage

Y. Zhou, S. P. Centeno, K. Zhang, L. Zheng, R. Göstl, A. Herrmann
DWI – Leibniz Institute for Interactive Materials
Forckenbeckstr. 50, 52056 Aachen, Germany
E-mail: goestl@dwi.rwth-aachen.de; herrmann@dwi.rwth-aachen.de
Y. Zhou, A. Herrmann
Zernike Institute for Advanced Materials
University of Groningen
Nijenborgh 4, Groningen 9747 AG, The Netherlands
K. Zhang, L. Zheng
Wenzhou Institute
University of Chinese Academy of Sciences
Wenzhou 325001, China
K. Zhang, A. Herrmann
Institute of Technical and Macromolecular Chemistry
RWTH Aachen University
Worringerweg 1, 52074 Aachen, Germany
The ORCID identification number(s) for the author(s) of this article can be found under https://doi.org/10.1002/adma.202210052.

DOI: 10.1002/adma.202210052

to the glued materials is monitored visually, by in situ fluorescence spectroscopy, and by fluorescence lifetime imaging microscopy (FLIM) identifying damage zones.

2. Results and Discussion

In previous work, we genetically engineered green fluorescence protein (GFP) to turn off its fluorescence upon force application by ultrasound (US).[23] By incorporating unfolded loop-forming supercharged polypeptides (SUPs) with the elastin-derived sequence $(VPGEG)_n$ into circularly permuted GFP (CpGFP), the shear force generated during sonication was transferred efficiently to the protein structure. Thereby, the hydrogen-bonding network around the GFP fluorophore with the β barrel was disturbed resulting in a decrease in GFP fluorescence. Based on this, we conducted further modifications to conceive a protein mechanophore using the CpGFP system.

We first inserted a $(VPGKG)_{72}$ SUP domain into the CpGFP with the mutations C48A, F64L, S65T, and Q204C resulting in the construct CpGFP-K72 (**Scheme 1**). The Cys-48 on the surface of GFP was mutated to alanine and a new cysteine residue was introduced to Gln-204 for site-specific chemical modification with a maleimide-functionalized complementary fluorophore to warrant high FRET efficiency.[48] We chose Atto 390 to react with the CpGFP-K72 to form the designed FRET pair CpGFP-K72-atto390, in which a green to blue fluorescence emission shift was expected upon force application based on biasing the distance between FRET donor and acceptor. Additionally to the CpGFP system, we synthesized both N- and C-terminal SUP-modified protein K36-GFP-K36-atto390 using the same strategy (**Figure 1**a).

After confirming the successful modification with Atto 390 by matrix-assisted laser desorption/ionization time-of-flight MS (MALDI-TOF-MS, Figure S2, Supporting Information), we first recorded the absorption and emission spectra of 10 μM protein solutions. From the absorption spectra, the average degrees of labeling (DOL, dye-to-protein ratio) of K36-GFP-K36-atto390 and CpGFP-K72-atto390 were determined to be 96% and 75%, respectively. High FRET efficiencies were also observed by exciting both FRET pairs at the excitation wavelength of Atto 390. To calculate the exact FRET efficiencies, we denatured the two conjugates at 98 °C thereby excluding intermolecular FRET that was not based on the spatial proximity of the dyes within the secondary structure of the protein. The resulting emission spectra were comparable to those of the donor in absence of the acceptor. Subsequently, the emission spectra of the pristine conjugates were recorded and the donor emission in presence of the acceptor was divided by the donor emission in absence of the acceptor to obtain the FRET efficiencies. (Figures S3, S4, Supporting Information).[49]

Hereafter, we sonicated CpGFP-K72-atto390 using an immersion probe sonicator (20 kHz). We found that the absorption band at 480 nm of the GFP fluorophore was reduced to 25% after 6 min while the 390 nm band of Atto 390 was not altered. Moreover, we found that the Atto 390 absorption band at 390 nm shifted to 385 nm, indicating a change in the local environment by solvatochromism.[50] The decreased GFP absorption was reflected in the emission spectra where at λ_{exc} = 340 nm the FRET acceptor GFP emission band decreased significantly together with an increase of the FRET donor Atto 390 emission band. These results underlined that CpGFP-K72-atto390 allowed successful FRET modulation of 30% decreasing FRET efficiency upon force application (Figure 1b,c). We observed similar effects using K36-GFP-K36-atto390 (Figure 1d,e). In earlier work, we found that this process was caused by partially reversible but also irreversible transitions and did not revert considerably on timescales required for optical analysis.[23] Since circular permutations would usually destabilize the secondary structure of the protein,[51] we hypothesized that CpGFP-K72-atto390 would show higher mechanochemical activity than K36-GFP-K36-atto390, which we demonstrated in the following lap shear tests (vide infra).

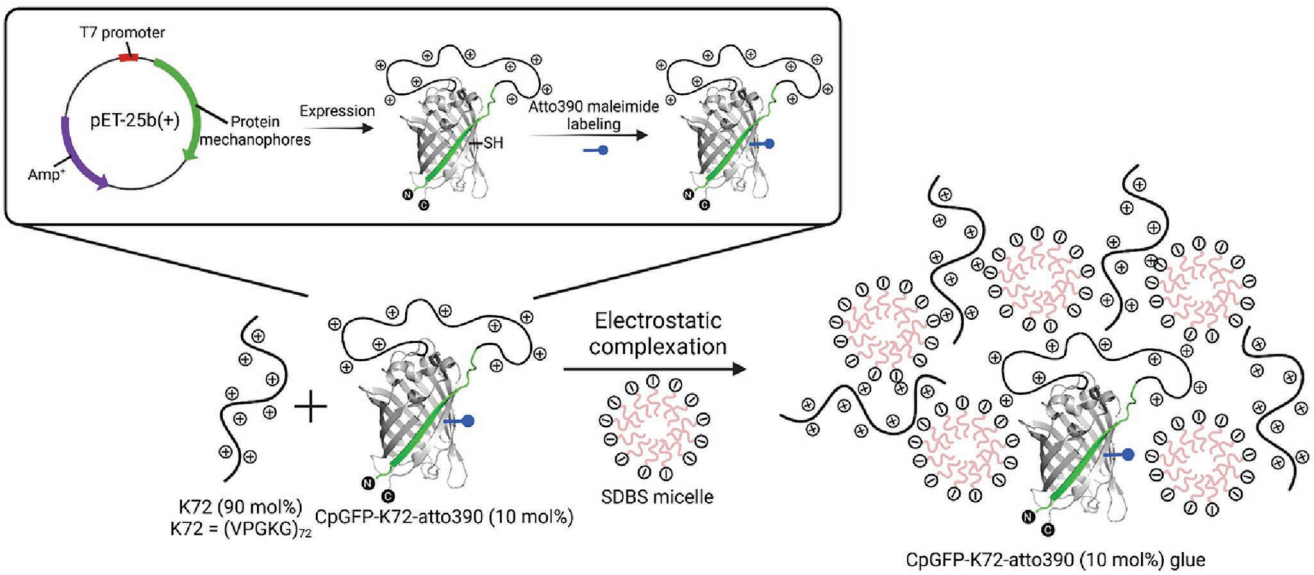

Scheme 1. Schematic representation of the expression of CpGFP-K72-atto390 and the formation of its corresponding glue (10 mol%). In this case, the composition of the protein component is 10 mol% CpGFP-K72-atto390 and 90 mol% K72.

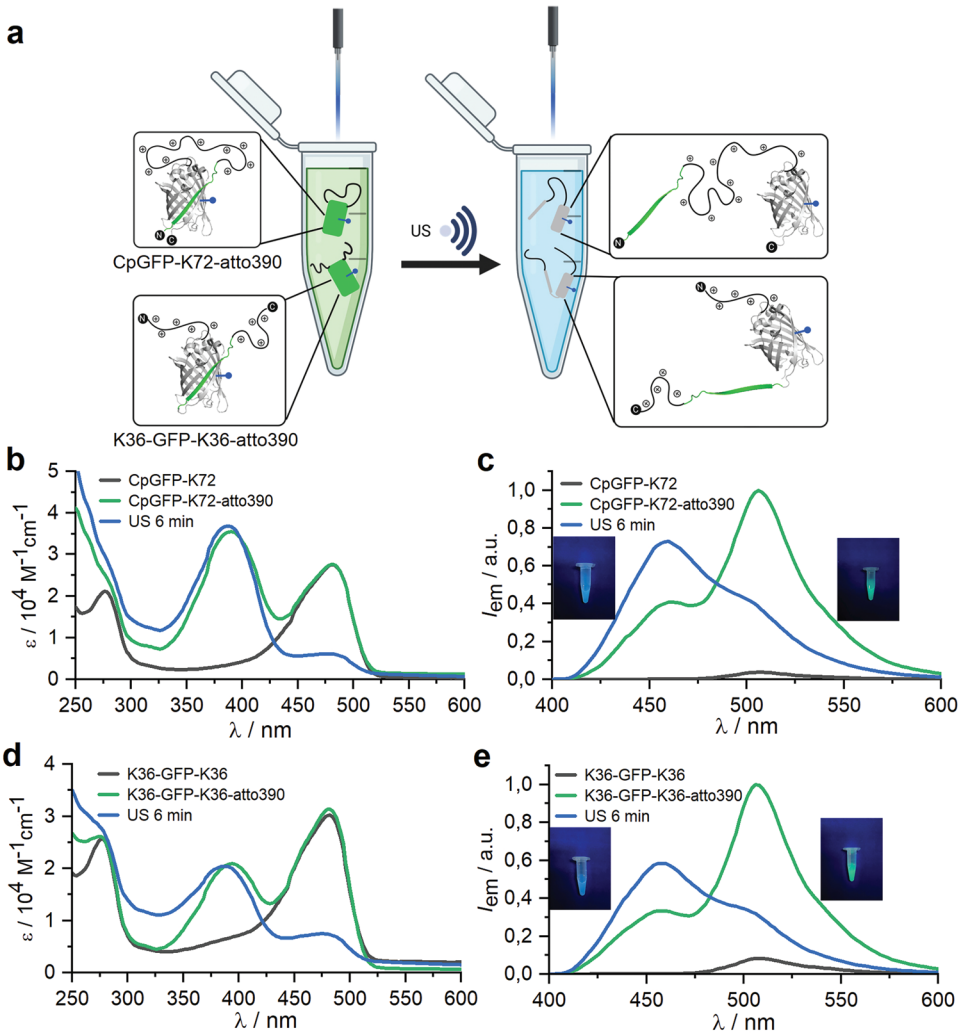

Figure 1. a) Schematic representation of US-induced protein mechanophore FRET variation. Both circular permuted CpGFP-K72-atto390 (top) and linear K36-GFP-K36-atto390 (bottom) release the GFP fluorophore from the β barrel upon mechanical stimulation in the form of US (left to right) thereby increasing FRET donor emission by Atto 390. b) Absorption spectra of CpGFP-K72 (black), CpGFP-K72-atto390 (green), and CpGFP-K72-atto390 after 6 min sonication (blue). c) Normalized (to maximum) emission spectra corresponding to (b). d) Absorption spectra of K36-GFP-K36 (black), K36-GFP-K36-atto390 (green), and K36-GFP-K36-atto390 after 6 min sonication (blue). e) Normalized (to maximum) emission spectra corresponding to (d). All spectra were measured in PBS buffer (pH 7.4) at room temperature, and protein concentrations were in the range of 10 µM. λ_{exc} = 340 nm.

Having established the principal function of the protein OFPs in solution, we sought to apply these to the mechanical failure detection of glues. Protein mechanophores and sodium dodecylbenzenesulfonate (SDBS) micelles were mixed in an aqueous solution in a 1:1 molar ratio of lysine units to surfactant. Flocculent precipitates were formed and afterward collected by centrifugation. The formation mechanism of such precipitates was recently reported by us.[46] Phase separation processes occurred when positively charged SUPs were brought into contact with the negatively charged SDBS yielding the complex coacervate (Scheme 1). Such coacervate adhesives are an emerging class of functional glues, particularly promising for biomedical applications due to their biocompatible and occasionally bioinstructive properties.[52,53]

After the glue complex was separated from the supernatant, lap shear tests were performed to characterize the mechanical gluing properties and to produce fracture surfaces. Glass was chosen as the high-surface-energy model substrate first.[54] The protein OFP–SDBS complexes were applied to the overlap area between two glass slides and cured at room temperature. The water content of the glue decreased along with the curing time, which correlated to the fracture strength.[46] Since the nearly dry glues were very tough leading to the fracturing of the glass substrate after mechanical loading, we reduced the necessary loading force to achieve glue failure by optimizing the curing time and thereby the water content. This was a compromise between the beneficial optical properties of the glass and the desire to probe the material under investigation. Under the preset water content, fracture strengths of 3.15 ± 0.42 MPa of pure CpGFP-K72-atto390 glue and 4.49 ± 0.92 MPa of pure K36-GFP-K36-atto390 glue were obtained in analogy to previously reported K72-SDBS glue (Figure S5, Supporting Information).[46]

Subsequently, we used a portable fluorimeter to characterize the fluorescence variation before and after lap shear testing

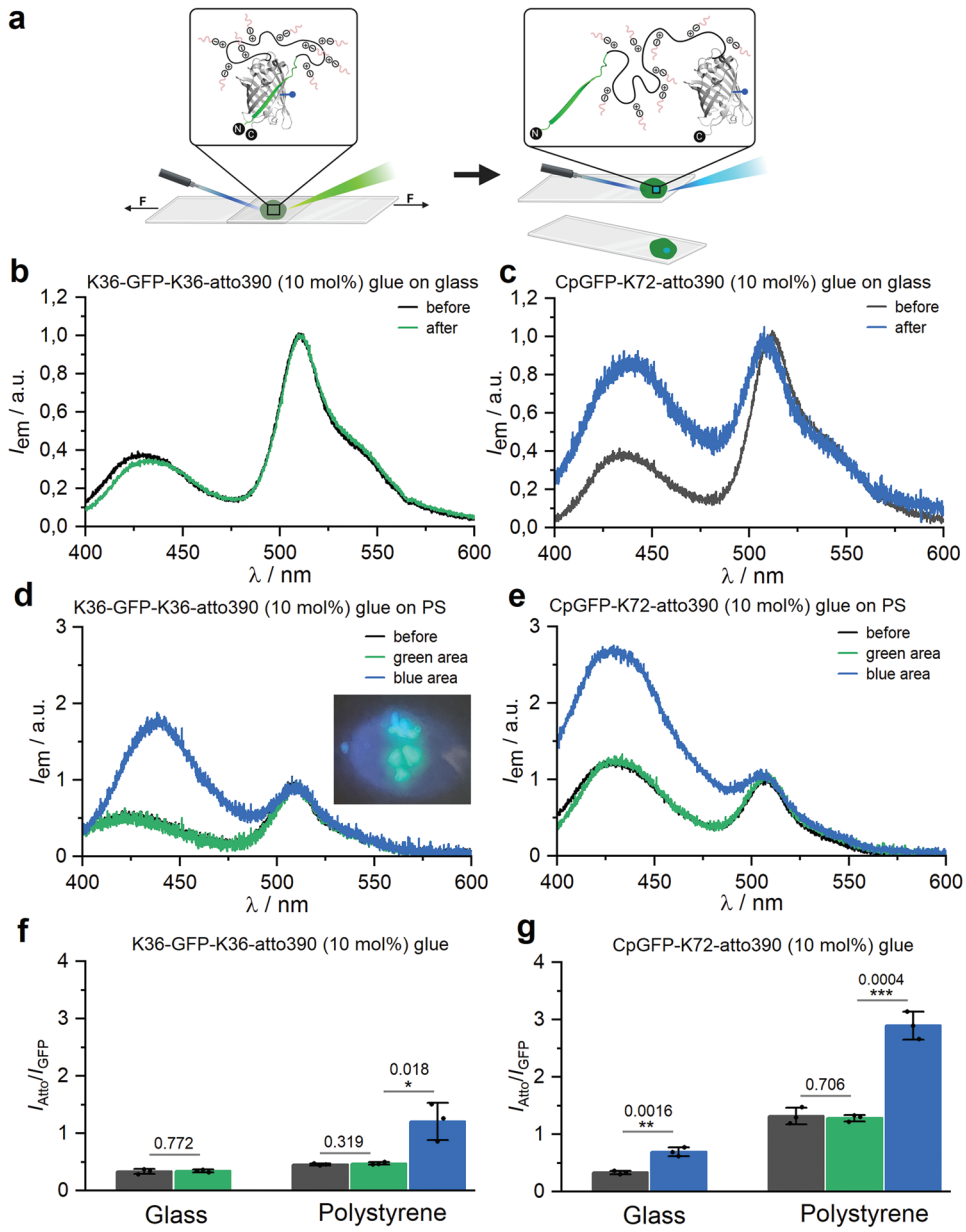

Figure 2. a) Schematic representation of protein mechanophore FRET variation during the lap shear tests. b) Normalized (to GFP) emission spectra of K36-GFP-K36-atto390 (10 mol%) glue bonding glass before (black) and after (green) lap shear tests. c) Normalized (to GFP) emission spectra of CpGFP-K72-atto390 (10 mol%) glue bonding glass before (black) and after (blue) lap shear tests. d) Normalized (to GFP) emission spectra of K36-GFP-K36-atto390 (10 mol%) glue bonding PS before (black) and after the lap shear tests. e) Normalized emission spectra of CpGFP-K72-atto390 (10 mol%) glue bonding PS before (black) and after lap shear tests. f) K36-GFP-K36-atto390 (10 mol%) glue only responded to adhesive failure. g) CpGFP-K72-atto390 (10 mol%) glue responded to both cohesive and adhesive failure. The data obtained from the PS samples (f,g) after lap shear testing was inhomogeneous and included unaltered zones (green) and damaged zones (blue). Mean values ± SD from the mean. $N = 3$ different lap shear tests. P-values calculated using Student's t-test (two-sided), $^{*}P < 0.05$, $^{**}P < 0.01$, $^{***}P < 0.001$.

(**Figure 2**a). Fluorescence emission spectra were obtained and normalized according to the GFP fluorescence intensity. As we hypothesized, the suspectedly less sensitive K36-GFP-K36-atto390 glue was not force responsive within the coacervate glues, but the CpGFP-K72-atto390 glue showed subtle differences (Figure S6, Supporting Information). The fluorescence intensity of Atto 390 increased slightly upon lap shear testing, indicating that a small population of CpGFP fluorophores was deactivated. However, the difference was insufficient for complete failure detection. We hypothesized that the fluorophore concentration played a critical role in the control of the sensitivity of the protein OFPs, because intermolecular FRET contributed significantly more to the overall observed FRET at high concentrations than intramolecular FRET, and the former would not correlate linearly with turning off GFP fluorescence.[55]

Thus, to minimize the effect of intermolecular FRET, we formed the glue using a lower concentration of fluorescent components by blending in pure SUP K72 $(VPGKG)_{72}$ to maintain the total lysine unit concentration. The glue composition was optimized to 10 mol% fluorescent components and 90 mol% K72 for all following measurements. At these conditions, the solid glue samples showed a similar level of FRET efficiency as the 10 μM protein-dye solution samples and fracture strengths comparable to the original fluorescent glues. The K36-GFP-K36-atto390 (10 mol%) glue maintained a consistent Atto 390 fluorescence intensity during tests (Figure 2b), while the CpGFP-K72-atto390 (10 mol%) glue showed a higher sensitivity toward force (Figure 2c). We chose three regions of interests (ROIs) on each slide for fluorescence measurements and at all ROIs I_{Atto}/I_{GFP}, indicative of force-induced GFP deactivation, increased from ≈0.4 to 0.9 (Figure 2g). This proved that the protein OFP system was not only applicable in solution but also reliable in solid materials.

Polystyrene (PS) was then selected for further exploration as low energy surface.[56] Compared to glass, PS exhibits a surface energy of 36 dyn cm^{-1}, which led to large contact angles between the PS surface and the hydrophilic glues. This caused PS to show very little attractive interaction, which is known for common adhesives.[57] Consequently, lap shear tests between low-energy surfaces and adhesives featured mostly adhesive failure, while on high-energy surfaces mainly cohesive failure was observed. The lap shear tests of K36-GFP-K36-atto390 (10 mol%) and CpGFP-K72-atto390 (10 mol%) glues on PS surfaces validated this interpretation. Adhesive failure was frequently observed and the measured fracture strengths of both types of glue were 1.76 ± 0.11 MPa and 0.88 ± 0.16 MPa, respectively (Figure S5, Supporting Information).

Notably, different patterns of fluorescent areas were identified among the remaining glue materials on the PS surface after fracture, independent of the employed glue. K36-GFP-K36-atto390 (10 mol%) glue was studied first with hardly any fluorescence changes in most cases. However, occasionally we observed non-homogenous FRET variations after lap shear testing. As shown in Figure 2d, most ROIs were emitting green fluorescence under excitation at 340 nm LED light with the exception of one blue fluorescent ROI. Emission spectra collected from the green ROIs were consistent with the spectra recorded before the lap shear tests, and the emission spectra in the blue ROI displayed a major peak ≈420 nm following a minor GFP emission peak. We repeated these experiments to exclude coincidental factors and the interference of possible autofluorescence of any of the used materials confirming that the increased peak at 420 nm originated from liberated Atto 390 and FRET dramatically decreased during lap shear tests in the blue ROI (Figure 2f). Comparable observations were made for the CpGFP-K72-atto390 (10 mol%) glue, and an even higher I_{Atto}/I_{GFP} was observed in the blue emitting areas because of the disappearance of the GFP emission (Figure 2e). These experiments indicated that the fracture of the glues was a highly localized and inhomogeneous process and motivated us to investigate the fracture process with higher spatial resolution.

Although the detection with the portable fluorimeter was fast and convenient, it was limited by the inherent spatial resolution of the device. Monitoring the ROIs on the microscale was therefore carried out by confocal laser scanning microscopy. Specifically, we used FLIM since the FRET process altered the fluorescence lifetime of the donor molecule. In addition, we considered FLIM-FRET to be a more robust method to evaluate FRET efficiencies since fluorescence lifetimes are independent of excitation intensity, dye concentration, and photobleaching (**Figure 3**a).[58,59] Despite its advantages, FLIM has found almost no application in conjunction with OFPs (with notable exceptions).[60,61] Since Atto 390 and GFP fluorescence overlapped substantially, Atto 390 could not be excited in our FLIM setup, and the force-induced modulation of the acceptor is a requirement for the FLIM-based analysis of the donor, we relied on a different set of FRET dyes. Therefore, we used existing fluorescent-protein FRET pairs, since the natively folded fluorescent proteins are more stable toward force than their circularly permuted versions. Thereby, fluorescent proteins were employed to replace the organic dye as a donor-yielding protein-protein OFPs. We used GFP and mCherry as established FRET pair[62] by fusing full-length superfolder GFP to the C-terminus of circularly permuted superfolder mCherry2 with a K72 loop to form CpCherry-K72-GFP (Figure S7, Supporting Information). Although recombinant expression and purification were convenient, the protein-protein OFPs exhibited a lower FRET efficiency because the maturation of mCherry2 was slow and likely rather inhibited by the presence of the supercharged K72 loop leading to a relatively decreased molar absorptivity of the fluorescent protein.

The corresponding CpCherry-K72-GFP (10 mol%) glue was fabricated analogously to the above and exhibited comparable adhesive properties with fracture strengths of 4.7 ± 0.97 and 1.82 ± 0.31 MPa on glass and PS, respectively (Figure S5, Supporting Information). A single superfolder GFP and CpCherry-K72 protein were produced and independently analyzed by FLIM as a control to confirm the individual FRET donor and acceptor fluorescence lifetimes. Superfolder GFP physisorbed on a cover glass exhibited an average amplitude-based lifetime τ_A and an intensity-based lifetime τ_I of 1.64 and 1.83 ns, respectively, at λ_{exc} = 488 nm excitation. The τ_A value is in the range of the expected lifetimes for GFP on a medium of high refraction index, such as the used glass. According to Davis, Suhling, and coworkers[63] for the dependence of the lifetime of GFP on the relative dielectric permittivity of the medium, we expected it also to be close to the average lifetime in the environment[64,65] of the coacervate glue. Therefore, in the following FRET studies, we used the amplitude-based lifetime on the glass as the average lifetime value for the free GFP donor in the glue environment. We used 488 nm excitation for detecting FRET donor GFP emission and 588 nm excitation for the FLIM of the acceptor force-sensitive CpCherry-K72. When physisorbed to glass, CpCherry-K72 had a τ_A of 1.04 ns (1.18 ns for τ_I) under 588 nm excitation (Figure S8, Supporting Information).

To achieve a good overview of the glued area, we used an HC PL FLUOTAR 5 ×/0.15 dry objective to observe the cured glue between the glass substrate and a microscopy cover slide without force application. CpCherry-K72-GFP (10 mol%) glue was distributed homogenously on the glass and by fitting the FLIM image, we estimated a $\tau_{A\text{-}GFP}$ of 0.58 ns (Figure 3b; Figure S9, Supporting Information), which was considerably

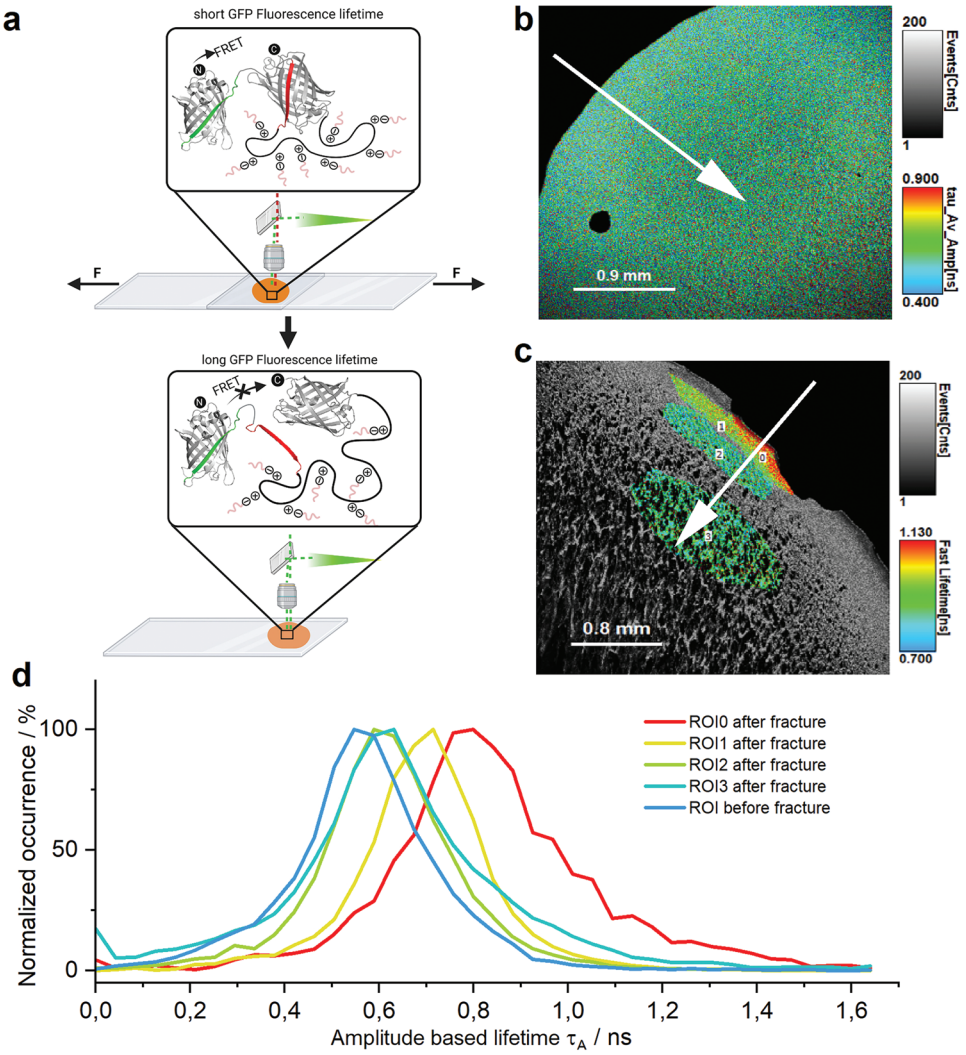

Figure 3. a) Schematic representation of protein mechanophore FRET variation detected by FLIM after lap shear test on two glued glass slides. b) FLIM map of GFP-CpCherry2-K72 (10 mol%) glue on glass before lap shear test with color coding. λ_{exc} = 488 nm. c) FLIM map of GFP-CpCherry2-K72 (10 mol%) glue on glass after lap shear test with color coding. λ_{exc} = 488 nm. d) Histogram of amplitude-based lifetime distribution from different ROIs, in which the ROIs of the sample after fracture (ROI 0–3) have been localized in (c).

shorter than the τ_A of 1.64 ns for the unmodified superfolder GFP fluorescence. This indicated a successful FRET from GFP to CpCherry-K72 and FRET within the glue.

The fractured glue sample was analyzed analogously. Different from the homogenous microscopy images before force application, in the FLIM images we observed a bulk area with an average lifetime $\tau_{A\text{-}GFP}$ of 0.66 ns that increased toward the fracture edges (Figure 3c; Figure S10, Supporting Information). Simultaneously, FRET efficiency images showed a clear shift from 66.7% to 61.7% before and after fracture (Figure S11, Supporting Information). The FLIM image of CpCherry-K72 by direct excitation at 588 nm was also recorded at the same location and the signal corresponding to the FRET acceptor vanished (Figure S12, Supporting Information). This underlined that the $\tau_{A\text{-}GFP}$ alterations were driven by the unfolding of acceptor CpCherry-K72. The microscopy images suggested that protein unfolding was strongest in the edge regions, which we interpreted as areas of stress accumulation during lap shear testing. We chose four representative ROIs together with one ROI from the sample without force application for comparison. The detailed ranges of all the ROIs and corresponding FLIM fittings are shown in Figure S13 (Supporting Information). ROI3 with a $\tau_{A\text{-}GFP}$ of 0.64 ns was measured within the central part of the glue surface, which should representatively depict glue failure within the bulk. ROI2 from an intermediate area and ROI1 from the edge region were then selected with $\tau_{A\text{-}GFP}$ of 0.62 and 0.71 ns respectively. Last, ROI0 was investigated due to its comparatively high $\tau_{A\text{-}GFP}$ of 0.80 ns. The amplitude-based lifetime histograms of those four ROIs were significantly different from the original lifetime before force application (Figure 3d), and the trend showed a decreasing fluorescence lifetime of the donor GFP from the edge to the central region.

In addition to the stress distribution in the *x*- and *y*-direction, we performed a *z*-stack of FLIM images with a *z*-step size of 10 µm to achieve a more complete and 3D spatial overview over glue failure (**Figure 4**a). Therefore, FLIM and FRET efficiency

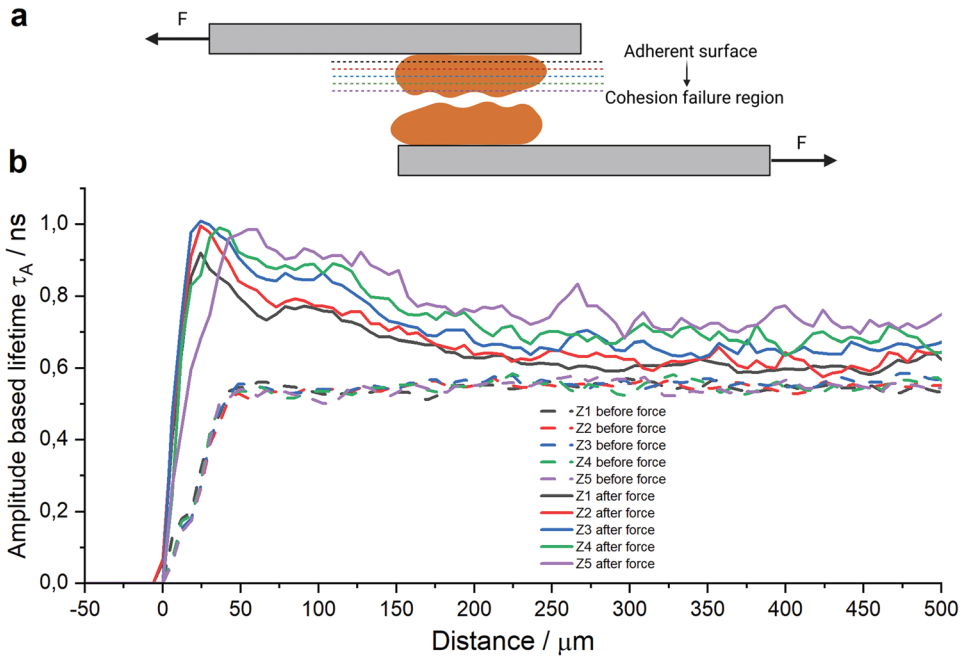

Figure 4. a) Schematic representation of FLIM measurements of different *z*-heights from the adherent part of GFP-CpCherry2-K72 (10 mol%) glue to the cohesive failure region. b) The comparative plot profiles of the amplitude-based lifetime from different *z*-height layers following the arrow in Figure 3b,c, and the zero points of the distance have been set to the edge of the glue samples.

images of the different *z*-axis levels of CpCherry-K72-GFP (10 mol%) glue before and after force application were acquired (Figures S14–S17, Supporting Information), and the $\tau_{A\text{-}GFP}$ data of every pixel following a straight line from the edge to the inner area were extracted as plot profile. As shown in Figure 4b, the curves of all five *z*-heights from the sample before the lap shear test exhibited identical profiles. The five layers from the fractured glue samples showed generally higher $\tau_{A\text{-}GFP}$ increasing toward the edge, as expected from the *xy*-microscopy images. Notably, $\tau_{A\text{-}GFP}$ was also increasing with *z*-height approaching the cohesive fracture zone. We thereby pinpointed the largest stress accumulation to those regions where the cohesive failure occurred and excluded adhesive failure in this specific test.

Subsequently, we conducted two additional replicate experiments with independently manufactured glue samples to assess the reproducibility of the observed effects. The first replicate was comparable to the initial experiment, except for a slightly different edge area (Figures S18–S20, Supporting Information). The increasing GFP amplitude-based lifetime in the *z*-stack FLIM images from the adherent surface to the cohesion failure region, and the decreasing fluorescence lifetime of the donor GFP from the area close to the edge to the central region both indicated a fracture mode similar to the initial experiment. More interestingly, the edge part of this second sample showed a relatively low GFP-amplitude-based lifetime on different *z*-heights of the FLIM images, which could stem from a mainly adhesive failure occurring in this zone. The second replicate glue sample likely contained less water than the first two samples and thus experienced a larger force application during the lap shear test. Hence, some comparatively high GFP amplitude-based lifetimes were observed on the different z-stack images (Figures S21–S23, Supporting Information). In general, the gluing process and fracture are both highly heterogeneous processes, but our OFP system could qualitatively localize stress distributions upon glue fracture by monitoring the OFP fluorescence lifetime.

3. Conclusion

We have presented a series of unprecedented protein OFPs by combining force-sensitive circularly permuted fluorescent proteins and corresponding FRET donors, which can be organic dyes or other fluorescent proteins. This OFP platform is highly flexible and tunable in its excitation and detection wavelengths as it draws from the vast pool of existing fluorescent proteins and small molecular dyes for FRET. We showed the principal working mechanism in solution by ultrasonication and then prepared force-responsive coacervate bio-glues using these mechanophores by electrostatic complexation of cationic polypeptides from the protein mechanophores and anionic aromatic surfactants. We then monitored stress-induced FRET alterations upon lap shear testing using solid-state fluorescence spectroscopy with ratiometric FRET pairs. Subsequently, we performed FLIM-FRET to achieve a spatially resolved 3D overview in *x*-, *y*-, and *z*-direction, thereby qualitatively localized stress distributions upon glue fracture, and differentiated cohesive from adhesive failure. We thereby developed an unprecedented methodology for the microscopy-based fractography of glues using principles of polymer mechanochemistry in combination with genetically engineered polypeptides and proteins. While individual pieces of information, such as the differentiation of adhesive and cohesive fracture or glue failure monitoring, can be obtained with existing methods, the OFP-based

glue fracture detection offers direct visual and spatial feedback over the mechanical state of the glue and may thereby expand the parameter space that can be investigated. However, current limitations, such as the incompatibility with traditional adhesives, the high probe content relative to the glue under investigation, and the optical incompatibility of tougher substrates, must be overcome to achieve this. In addition, challenges to obtain quantitative fracture information using FRET and FLIM-FRET must be overcome.

4. Experimental Section

Materials: Reagents were of analytical grade and used without further purification. Tryptone and yeast extract used for Terrific Broth (TB) medium were purchased from Duchefa. T4 DNA ligase (5 Weiss U μL^{-1}) was purchased from Thermo Fisher Scientific. RotiGelStain was received from Carl Roth (Germany). Atto 390 maleimide dye was purchased from Atto-tec (Germany). Glass microscope slides and cover slips were purchased from VWR. Super-DHB was used as a matrix during MALDI-TOF MS and was purchased from Merck. Miscellaneous chemicals were purchased from Sigma Aldrich unless otherwise noted. MilliQ water with a resistivity of >18.2 MΩ cm was used for all experiments.

Molecular Cloning: CpGFP and GFP-CpsfCherry2 backbone fragments (Figure S1, Supporting Information) with the recognition sites of the restriction enzymes PflMI and BglI were ordered (IDT). The fragments were ligated to pJET 1.2 blunt vector using T4 DNA ligase according to the blunt-end ligation protocol; the DNA fragment was used in a 3:1 molar ratio with pJET1.2/blunt vector, and the ligation mixture was transformed directly after 15 min at 22 °C incubation. Because BglI was used in further cloning, the present BglI site on the pJET vector was removed using the primers FW: 5′-CGC CGA GCG CAG AAG TGG TC-3′ and RV: 5′-CTG CCG GCT GGC TGG TTT ATT G-3′. pJET-CpGFP and pJET- GFP-CpsfCherry2 were constructed in this manner.

The building block of the cationic ELP gene (K36) on PUC19 was constructed previously by this group.[66] The K36 gene was cut from the PUC19 vector by digestion with PflMI and BglI and run on a 1% agarose gel in TAE buffer. The band containing the K36 gene was excised from the gel and purified using a spin column purification kit (General Electric). pJET with target fragments were also digested with PflMI and BglI and dephosphorylated with Fast AP. The vectors were purified by 1% agarose gel extraction. The linearized pJET vectors and the K36-encoding gene were ligated using T4 ligase with a molar ratio of 1:3 and transformed into chemically competent DH5α cells. Cells were plated and colonies were picked and grown in LB medium supplemented with 100 $\mu g\ mL^{-1}$ carbenicillin overnight, and plasmids were isolated using the GeneJET Plasmid Miniprep kit. Positive clones were verified by analytical digest with PflMI and BglI following gel electrophoresis. The DNA sequences of the inserts were verified by DNA sequencing (Microsynth Sequencing AG). Gene oligomerization was performed as described by Chilkoti and co-workers.[67] Finally, the gene fragments encoding the ELP fusion proteins were transferred into the expression vector pET25b(+) for protein expression.

Protein Expression and Purification: *E. coli*. BLR(DE3) (Novagen) was chosen as the expression strain because this strain stabilizes plasmids with repetitive sequences. For protein production, overnight culture was diluted 1/100 in TB medium supplemented with 100 $\mu g\ mL^{-1}$ carbenicillin and incubated at 37 °C shaking at 200 rpm until OD_{600} ≈0.8–1.0. Protein production was initiated with 1 mM IPTG at 22 °C for at least 16 h. Cells were subsequently harvested by centrifugation (6000 × g, 20 min, 4 °C), resuspended in lysis buffer (50 mM phosphate buffer, pH 8.0, 300 mM NaCl, 20 mM imidazole, 0.5 mM PMSF, 10 $\mu g\ mL^{-1}$ DNaseI) and disrupted by high-pressure homogenizer (Constant Systems Ltd Muti-Shot). Insoluble cell debris was removed by centrifugation (15 000 × g, 30 min, 4 °C). Proteins were purified from the supernatant under native conditions by Ni-sepharose chromatography: Supernatant was filtered using a 0.22 µm pore size membrane filter (Millipore Corp.), and loaded onto a Histrap fast flow column (General Electric), pre-equilibrated with His-binding buffer (50 mM phosphate buffer, 500 mM NaCl, 20 mM Imidazole, pH 7.4). Next, 5–8 column volumes of His-washing buffer (50 mM phosphate buffer, 500 mM NaCl, 50 mM imidazole, pH 7.4) were added to remove impurities, after which 3 column volumes of His-elution buffer (50 mM phosphate buffer, 500 mM NaCl, 500 mM imidazole, pH 7.4) were used to collect the target protein. The product was further purified by ion exchange chromatography (heparin HP column for lysine-containing SUPs). To this end, the product was 10× diluted with 50 mM phosphate buffer (pH 8) and loaded onto a pre-equilibrated (IEC A buffer: 50 mM phosphate buffer, 20 mM NaCl, pH 8) ion exchange column. The supercharged target protein was purified with a 10-column volumes gradient elution program from 100% IEC A buffer to 100% IEC B (50 mM phosphate buffer, 2 M NaCl, pH 8) buffer with a flow speed of 0.5 mL min^{-1}. Finally, the pure products were desalted by using Pierce Protein Concentrators PES, 3K MWCO (ThermoFisher) with milliQ water and then were frozen in liquid N_2, lyophilized, and stored at −80 °C for further usage.

Characterization of SUPs: The concentrations of the purified ELP fusion proteins were determined by absorbance at 280 nm using a NanoDrop One microvolume UV–vis spectrophotometer (ThermoFisher). Protein purity was determined on a 15% SDS-PAGE stained with Coomassie staining solution (40% MeOH, 10% glacial AcOH, 1 g L^{-1} brilliant blue R250), and analyzed with ImageJ software. Photographs of the gels were taken with a Bio-Rad gel imager (E-box, Vilber). The resulting stained Gel was shown in Figure S1 (Supporting Information), and the SUPs present different electrophoretic mobility according to their molar mass and charge (Table S1, Supporting Information).

MALDI-TOF MS was carried out on a Bruker Daltonics ultrafleXtreme. The protein samples were mixed 1:1 v/v with a matrix solution of 50 mg mL^{-1} SDHB in TA50 solvent (50:50 [v/v] MeCN:0.1% TFA in H_2O). Mass spectra were analyzed with the Data Explorer software (version 4.9) and the data were plotted with Origin Pro 9.1. Values determined by mass spectrometry were in good agreement with the masses that were calculated (Figure S2, Table S1, Supporting Information) based on the amino acid sequence.

Protein-Dye Conjugation: Conjugation was performed according to the Thiol-Reactive ATTO-Label (Maleimides) protocol from Atto-tec. A reactive dye solution was prepared by dissolving 1.0 mg of dye-maleimide in 50–200 µL of anhydrous, amine-free DMF. Free thiol from the protein of interest (1–5 mg mL^{-1} in PBS, pH 7.4) was reacted with dye-maleimide by adding a 1.3 molar excess of reactive dye per sulfhydryl group while gently shaking. The reaction mixture was protected from light for 2 h at room temperature. Free unbound dye was removed by centrifugation with a Pierce Protein Concentrator PES, 3k MWCO (3×). Purified conjugates were frozen in liquid N_2, lyophilized, and stored at −80 °C for further usage.

The average degree of labeling (DOL, dye-to-protein ratio) was calculated by the following formula:

$$\mathrm{DOL} = \frac{c_{\mathrm{dye}}}{c_{\mathrm{protein}}} = \frac{A_{\mathrm{dye,max}} \cdot \varepsilon_{\mathrm{protein}}}{\left(A_{280} - A_{\mathrm{dye,max}} \cdot f_{280}\right) \cdot \varepsilon_{\mathrm{dye,max}}} \quad (1)$$

in which, $A_{\mathrm{dye,max}}$ is the absorbance at the dye absorption maximum, A_{280} is the absorbance at 280 nm, $\varepsilon_{\mathrm{protein}}$ is the molar absorptivity of the protein at 280 nm, $\varepsilon_{\mathrm{dye,max}}$ is the molar absorptivity of the dye at the dye absorption maximum, and f_{280} is the correction factor given by Atto-tec.

Preparation of SUP Glues: The SUP glues were prepared according to the previous work.[46] Briefly, an aqueous solution of the SUP with a concentration of ≈2.5 mM (K72, K36-GFP-K36-atto390, CpGFP-K72-atto390, and GFP-CpsfCherry2-K72) was obtained by dissolving the lyophilized SUP in milliQ H_2O. In a second solution made from milliQ water, the concentration of SDBS lipid was adjusted to 180 mM at room temperature. Fluorescent SUP solution was added into K72 solution to obtain the ratio predetermined complex solution, for example, 2 µL of 2.5 mM CpGFP-K72-atto390 solution was added to 18 µL of 2.5 mM K72 solution to prepare the 10 mol% CpGFP-K72-atto390 complex

solution. Both the complex solution and the SDBS solution were combined in a 1:1 molar ratio so that ≈1 mol of surfactant equals 1 mol of lysine residues within the SUP. After centrifugation, the SUP-SDBS complex sediments at the bottom of the vial as a coacervate and were separated from the aqueous supernatant. The supernatant was removed by a pipette and the SUP-SDBS glue material was collected.

Optical Experiments: A Microplate Reader Spectrophotometer (Molecular Devices SpectraMax M3) was used for all liquid absorbance and fluorescence measurements at room temperature in PBS (pH 7.4), and protein concentrations were in the 10 µM range. 340 nm was chosen as the excitation wavelength for K36-GFP-K36-atto390 and CpGFP-K72-atto390, and 488 nm was chosen for GFP-CpCherry2-K72.

Fluorescence emission spectra of the SUP glues were collected with a compact CCD spectrometer (CCS200, Thorlabs). A fiber-coupled LED (M340F3, Thorlabs) was used as a light source. The emission data was recorded by a fiber Y-bundle reflection probe (RP24, Thorlabs), which also transmitted the excitation light. Finally, the spectra were analyzed with the Thorlabs OSA software (version 2.90).

Sonication: A QSonica sonicator (20 kHz) was used. A 422-A probe (50% amplitude) was used for all sonication experiments. The program was a loop with 2 s on following 1 s off. Everything used for sonication was pre-cooled on ice and the 1.5 mL Eppendorf tubes containing 500 µL of the samples were placed in an ice-water bathed steel container during sonication.

Lap Shear Tests: Lap shear tests were carried out on two substrates, glass and PS. Glass microscope slides (75 × 25 × 0.5 mm) and cover slips (25 × 25 mm) were purchased from VWR. PS microscope slides (75 × 25 mm) were purchased from ThermoFisher. After adding the glue onto one slide, a second slide was then placed atop the first one to create a lap shear joint with an overlap area of 25 × 25 mm. The slides were then allowed to cure for 12 h at room temperature. Office clamps were used to hold the slides together during the curing period.

Lap shear tests were performed on a Zwick Roell testControl II equipped with a 5 kN load cell, at a loading rate of 50 mm min^{-1}. The bonding strength for each trial was obtained by dividing the maximum load (kN) observed at bond failure by the area of the adhesive overlap (m^2), giving the bonding strength in MPa (1000 kN m^{-2}). Each sample has tested a minimum of 3×.

FLIM: FLIM was performed with the single photon counting method by using an inverted confocal laser scanning microscope TCS SP8 X (Leica) equipped with an HC PL FLUOTAR 5 × /0.15 dry objective, two HyD SMD detectors (Leica), a PicoHarp 300 TCSPC Module, a PHR 800 Router (PicoQuant) and a supercontinuum White Light Lasers (Leica). Each image was acquired at a fixed *z*-position in the sample and consisted of 512 × 512 pixels with a pixel size of 6 µm. The excitation power reaching the objective was ≈50 µW and the scanning speed was set to 4.8 µs $pixel^{-1}$ with an integration time of 50 frames per image. GFP fluorescence emission (500–550 nm) excited at 488 nm and mCherry fluorescence emission (630–700 nm) excited at 588 nm were collected through a 70 µm pinhole. Detected photons were registered with the high-speed PicoHarp 300 timing electronics and SymPhoTime 64 software (PicoQuant) in time-tagged time-resolved mode.

The fluorescence decay data were exclusively analyzed with the SymPhoTime 64 software, being the *n*-exponential reconvolution method used as the fitting model. The IRF used for deconvolution was the theoretical IRF estimated by the SymPhoTime 64 software. For the GFP physisorbed on glass, the fluorescence decay (1.7×10^6 photons) was fitted to a two components exponential function with a short lifetime component τ_1 amounting to 1.20 ns and characterized by an amplitude a_1 of 9.30 kcounts and intensity of 667 kcounts and a longer lifetime component τ_2 amounting to 2.26 ns and characterized by an amplitude a_2 of 7.30 kcounts and intensity of 1028 kcounts, respectively. This resulted in an estimated average amplitude-based lifetime and an intensity-based lifetime of 1.64 and 1.83 ns, respectively. The amplitude-based lifetime on glass was used as the average lifetime value for the free GFP donor in the glue environment for the estimation of the FRET efficiency. The CpCherry-K72 fluorescence decay (6×10^5 photons) excited at 588 nm was also fitted to a two components exponential function with a short lifetime component τ_1 amounting to 0.33 ns and characterized by an amplitude a_1 of 7.60 kcounts and intensity of 594 kcounts and a longer lifetime component τ_2 amounting to 1.25 ns and characterized by an amplitude a_2 of 2.20 kcounts and intensity of 44 kcounts, respectively. This resulted in an average amplitude-based lifetime τ_A of 1.04 ns (1.18 ns for the intensity-based lifetime).

For the bio-glue coacervate system the fluorescence decay (typically 6–200 × 10^5 photons) excited at 488 nm was fitted to an exponential function with 3 components with values amounting to ≈0.4, 0.9, and 1.8 ns, respectively, and whose amplitudes and intensities changed with the mechanical stress applied to the sample and with the ROI selected in the fractured sample. The number of components was exclusively selected by a low χ^2 and the scattering of the residuals and no further investigation was carried out in order to clarify the origin of each component. The different amplitudes of these components observed for the different samples were used to estimate the average amplitude-based lifetime and for plotting the FRET images and estimating the FRET efficiencies *E* by the SimPhoTime 64 software by the formula:

$$E = 1 - \frac{\tau_{DA,Amp}}{\tau_{D,Amp}} \quad (2)$$

where $\tau_{DA,Amp}$ is the amplitude-weighted average lifetime of the donor in the presence of the acceptor and $\tau_{D,Amp}$ is the amplitude-weighted average lifetime of the individual donor without the acceptor.

Statistical Analysis: For the study of adhesion strengths, all experiments were presented as mean ± SD from $N = 3$ independent measurements on independent samples. Origin software package (version 2022b) was used for the statistical analysis with Student's *t*-test (two-sided) between two groups comparison. In all cases, a *P*-value less than 0.05 was considered to be statistically significant, $^*P < 0.05$, $^{**}P < 0.01$, $^{***}P < 0.001$, $^{****}P < 0.0001$. The SymPhoTime 64 software (PicoQuant) and ImageJ software were used for FLIM measurements analysis.

Supporting Information

Supporting Information is available from the Wiley Online Library or from the author.

Acknowledgements

Y.Z. was supported by the China Scholarship Council. R.G. is grateful for support from the German Research Foundation DFG through the Heisenberg Programme (503981124). A.H. thanks the German Research Foundation DFG (464907394). A.H. and R.G. acknowledge the Competence Center Bio4MatPro of the German Federal Ministry of Education and Research BMBF (031B1148A). Parts of the analytical investigations were performed at the Center for Chemical Polymer Technology CPT, which was supported by the European Commission and the federal state of North Rhine-Westphalia (300088302).

Open access funding enabled and organized by Projekt DEAL.

Conflict of Interest

The authors declare no conflict of interest.

Author Contributions

A.H., R.G., and Y.Z. designed the study. Y.Z. performed all experiments. K.Z. and L.Z. provided reagents and advice. S.P.C. performed the FLIM measurements. Y.Z., S.P.C., and R.G. analyzed and interpreted data. Y.Z.,

S.P.C., R.G., and A.H. designed figures and wrote the manuscript as well as the revision.

Data Availability Statement

The data that support the findings of this study are available from the corresponding author upon reasonable request.

Keywords

fluorescence lifetimes, optical force probes, polymer mechanochemistry, proteins

Received: October 31, 2022
Revised: January 25, 2023
Published online: March 11, 2023

[1] (Ed.: R. D. Adams), *Adhesive Bonding: Science, Technology and Applications*, 2nd ed., Woodhead Publishing, Oxford, UK **2021**.
[2] N. Annabi, Y.-N. Zhang, A. Assmann, E. S. Sani, G. Cheng, A. D. Lassaletta, A. Vegh, B. Dehghani, G. U. Ruiz-Esparza, X. Wang, S. Gangadharan, A. S. Weiss, A. Khademhosseini, *Sci. Transl. Med.* **2017**, *9*, aai7466.
[3] H. Yuk, J. Wu, T. L. Sarrafian, X. Mao, C. E. Varela, E. T. Roche, L. G. Griffiths, C. S. Nabzdyk, X. Zhao, *Nat. Biomed. Eng.* **2021**, *5*, 1131.
[4] J. Li, A. D. Celiz, J. Yang, Q. Yang, I. Wamala, W. Whyte, B. R. Seo, N. V. Vasilyev, J. J. Vlassak, Z. Suo, D. J. Mooney, *Science* **2017**, *357*, 378.
[5] B. Sharma, S. Fermanian, M. Gibson, S. Unterman, D. A. Herzka, B. Cascio, J. Coburn, A. Y. Hui, N. Marcus, G. E. Gold, J. H. Elisseeff, *Sci. Transl. Med.* **2013**, *5*, 167ra6.
[6] M. R. Prausnitz, R. Langer, *Nat. Biotechnol.* **2008**, *26*, 1261.
[7] J. Li, D. J. Mooney, *Nat. Rev. Mater.* **2016**, *1*, 16071.
[8] M. Farahani, A. Shafiee, *Adv. Healthcare Mater.* **2021**, *10*, 2100477.
[9] S. Ebnesajjad, C. F. Ebnesajjad in *Surface Treatment of Materials for Adhesive Bonding*, William Andrew Publishing, Oxford, UK **2014**, pp. 77–91.
[10] R. T. O'Neill, R. Boulatov, *Nat. Rev. Chem.* **2021**, *5*, 148.
[11] Y. Chen, G. Mellot, D. van Luijk, C. Creton, R. P. Sijbesma, *Chem. Soc. Rev.* **2021**, *50*, 4100.
[12] S. He, M. Stratigaki, S. P. Centeno, A. Dreuw, R. Göstl, *Chem. - Eur. J.* **2021**, *27*, 15889.
[13] H. Traeger, D. J. Kiebala, C. Weder, S. Schrettl, *Macromol. Rapid Commun.* **2021**, *42*, 2000573.
[14] C. Löwe, C. Weder, *Adv. Mater.* **2002**, *14*, 1625.
[15] D. A. Davis, A. Hamilton, J. Yang, L. D. Cremar, D. Van Gough, S. L. Potisek, M. T. Ong, P. V. Braun, T. J. Martínez, S. R. White, J. S. Moore, N. R. Sottos, *Nature* **2009**, *459*, 68.
[16] E. Ducrot, Y. Chen, M. Bulters, R. P. Sijbesma, C. Creton, *Science* **2014**, *344*, 186.
[17] M. Raisch, W. Maftuhin, M. Walter, M. Sommer, *Nat. Commun.* **2021**, *12*, 4243.
[18] H. Traeger, Y. Sagara, D. J. Kiebala, S. Schrettl, C. Weder, *Angew. Chem., Int. Ed.* **2021**, *60*, 16191.
[19] K. Makyła, C. Müller, S. Lörcher, T. Winkler, M. G. Nussbaumer, M. Eder, N. Bruns, *Adv. Mater.* **2013**, *25*, 2701.
[20] S. Lörcher, T. Winkler, K. Makyła, C. Ouellet-Plamondon, I. Burgert, N. Bruns, *J. Mater. Chem. A* **2014**, *2*, 6231.
[21] J. N. Brantley, C. B. Bailey, J. R. Cannon, K. A. Clark, D. A. Vanden Bout, J. S. Brodbelt, A. T. Keatinge-Clay, C. W. Bielawski, *Angew. Chem., Int. Ed.* **2014**, *53*, 5088.
[22] T. Stauch, M. T. Hoffmann, A. Dreuw, *ChemPhysChem* **2016**, *17*, 1486.
[23] Y. Zhou, S. Huo, M. Loznik, R. Göstl, A. J. Boersma, A. Herrmann, *Angew. Chem., Int. Ed.* **2021**, *60*, 1493.
[24] C. Grashoff, B. D. Hoffman, M. D. Brenner, R. Zhou, M. Parsons, M. T. Yang, M. A. McLean, S. G. Sligar, C. S. Chen, T. Ha, M. A. Schwartz, *Nature* **2010**, *466*, 263.
[25] D. R. Stabley, C. Jurchenko, S. S. Marshall, K. S. Salaita, *Nat. Methods* **2012**, *9*, 64.
[26] M. Morimatsu, A. H. Mekhdjian, A. S. Adhikari, A. R. Dunn, *Nano Lett.* **2013**, *13*, 3985.
[27] A. Freikamp, A. Mehlich, C. Klingner, C. Grashoff, *J. Struct. Biol.* **2017**, *197*, 37.
[28] R. Göstl, J. M. Clough, R. P. Sijbesma, in *Mechanochemistry in Materials*, Royal Society Of Chemistry, **2017**, pp. 53–75.
[29] M. Stratigaki, C. Baumann, L. C. A. van Breemen, J. P. A. Heuts, R. P. Sijbesma, R. Göstl, *Polym. Chem.* **2020**, *11*, 358.
[30] J. Slootman, V. Waltz, C. J. Yeh, C. Baumann, R. Göstl, J. Comtet, C. Creton, *Phys. Rev. X* **2020**, *10*, 041045.
[31] T. Matsuda, R. Kawakami, T. Nakajima, J. P. Gong, *Macromolecules* **2020**, *53*, 8787.
[32] C. Baumann, M. Stratigaki, S. P. Centeno, R. Göstl, *Angew. Chem., Int. Ed.* **2021**, *60*, 13287.
[33] Y. Chen, G. Sanoja, C. Creton, *Chem. Sci.* **2021**, *12*, 11098.
[34] X. P. Morelle, G. E. Sanoja, S. Castagnet, C. Creton, *Soft Matter* **2021**, *17*, 4266.
[35] G. E. Sanoja, X. P. Morelle, J. Comtet, C. J. Yeh, M. Ciccotti, C. Creton, *Sci. Adv.* **2021**, *7*, abg9410.
[36] M. Stratigaki, C. Baumann, R. Göstl, *Macromolecules* **2022**, *55*, 1060.
[37] J. Slootman, C. J. Yeh, P. Millereau, J. Comtet, C. Creton, *Proc. Natl. Acad. Sci. USA* **2022**, *119*, e2116127119.
[38] E. Izak-Nau, S. Braun, A. Pich, R. Göstl, *Adv. Sci.* **2022**, *9*, 2104004.
[39] S. J. Marshall, S. C. Bayne, R. Baier, A. P. Tomsia, G. W. Marshall, *Dent. Mater.* **2010**, *26*, e11.
[40] J. Renart, J. Costa, C. Sarrado, S. Budhe, A. Turon, A. Rodríguez-Bellido, in *Fatigue and Fracture of Adhesively-Bonded Composite Joints* (Ed.: A. P. Vassilopoulos), Woodhead Publishing, Amsterdam, The Netherlands **2015**, pp. 121–147.
[41] W. J. Van Ooij, A. Kleinhesselink, S. R. Leyenaar, *Surf. Sci.* **1979**, *89*, 165.
[42] M. J. Walzak, R. Davidson, M. Biesinger, *J. Mater. Eng. Perform.* **1998**, *7*, 317.
[43] A. M. Belu, D. J. Graham, D. G. Castner, *Biomaterials* **2003**, *24*, 3635.
[44] M. Ezrin, G. Lavigne, *Eng. Failure Anal.* **2005**, *12*, 851.
[45] R. Bhargava, S.-Q. Wang, J. L. Koenig, in *Liquid Chromatography / FTIR Microspectroscopy / Microwave Assisted Synthesis*, Springer, Berlin/Heidelberg, Germany **2003**, pp. 137–191.
[46] C. Ma, J. Sun, B. Li, Y. Feng, Y. Sun, L. Xiang, B. Wu, L. Xiao, B. Liu, V. S. Petrovskii, Bin Liu, J. Zhang, Z. Wang, H. Li, L. Zhang, J. Li, F. Wang, R. Göstl, I. I. Potemkin, D. Chen, H. Zeng, H. Zhang, K. Liu, A. Herrmann, *Nat. Commun.* **2021**, *12*, 3613.
[47] L. Xiao, Z. Wang, Y. Sun, B. Li, B. Wu, C. Ma, V. S. Petrovskii, X. Gu, D. Chen, I. I. Potemkin, A. Herrmann, H. Zhang, K. Liu, *Angew. Chem., Int. Ed.* **2021**, *60*, 12082.
[48] S. C. Reddington, E. M. Tippmann, D. D. Jones, *Chem. Commun.* **2012**, *48*, 8419.
[49] C. Berney, G. Danuser, *Biophys. J.* **2003**, *84*, 3992.
[50] A. Marini, A. Muñoz-Losa, A. Biancardi, B. Mennucci, *J. Phys. Chem. B* **2010**, *114*, 17128.
[51] G. S. Baird, D. A. Zacharias, R. Y. Tsien, *Proc. Natl. Acad. Sci. USA* **1999**, *96*, 11241.
[52] S. Chen, Q. Guo, J. Yu, *Aggregate* **2022**, *3*, e293.

[53] W. C. Blocher, S. L. Perry, *Wiley Interdiscip. Rev.: Nanomed. Nanobiotechnol.* **2017**, *9*, e1442.
[54] *Adhesion and Adhesives: Science and Technology* (Ed: A. J. Kinloch), Springer, Dordrecht, The Netherlands **1987**.
[55] Á. I. Fábián, T. Rente, J. Szöllősi, L. Mátyus, A. Jenei, *ChemPhysChem* **2010**, *11*, 3713.
[56] J. Höpken, M. Möller, *Macromolecules* **1992**, *25*, 1461.
[57] D. E. Packham, *Int. J. Adhes. Adhes.* **2003**, *23*, 437.
[58] P. G. Wu, L. Brand, *Anal. Biochem.* **1994**, *218*, 1.
[59] A. Zeug, A. Woehler, E. Neher, E. G. Ponimaskin, *Biophys. J.* **2012**, *103*, 1821.
[60] J. W. Woodcock, R. J. Sheridan, R. Beams, S. J. Stranick, W. F. Mitchell, L. C. Brinson, V. Gudapati, D. Hartman, A. Vaidya, J. W. Gilman, G. A. Holmes, *Compos. Sci. Technol.* **2020**, *192*, 108074.
[61] L. Michels, V. Gorelova, Y. Harnvanichvech, J. W. Borst, B. Albada, D. Weijers, J. Sprakel, *Proc. Natl. Acad. Sci. USA* **2020**, *117*, 18110.
[62] B. T. Bajar, E. S. Wang, S. Zhang, M. Z. Lin, J. Chu, *Sensors* **2016**, *16*, 1488.
[63] K. Suhling, J. Siegel, D. Phillips, P. M. W. French, S. Lévêque-Fort, S. E. D. Webb, D. M. Davis, *Biophys. J.* **2002**, *83*, 3589.
[64] T. L. McMeekin, M. Wilensky, M. L. Groves, *Biochem. Biophys. Res. Commun.* **1962**, *7*, 151.
[65] J. Babul, E. Stellwagen, *Anal. Biochem.* **1969**, *28*, 216.
[66] A. Kolbe, L. L. del Mercato, A. Z. Abbasi, P. Rivera Gil, S. J. Gorzini, W. H. C. Huibers, B. Poolman, W. J. Parak, A. Herrmann, *Macromol. Rapid Commun.* **2011**, *32*, 186.
[67] J. R. McDaniel, J. A. MacKay, F. G. Quiroz, A. Chilkoti, *Biomacromolecules* **2010**, *11*, 944.